Ionic Determinants of Functional Reentry in a 2-D Model of Human Atrial Cells During Simulated Chronic Atrial Fibrillation

Sandeep V. Pandit,* Omer Berenfeld,* Justus M. B. Anumonwo, Roman M. Zaritski,† James Kneller,‡ Stanley Nattel,‡ and José Jalife*

*Institute for Cardiovascular Research and Department of Pharmacology, State University of New York Upstate Medical University, Syracuse, New York; †Department of Computer Science, Montclair State University, New Jersey; and ‡Montreal Heart Institute, University of Montreal, Montreal, Quebec, Canada H1T 1C8

ABSTRACT Recent studies suggest that atrial fibrillation (AF) is maintained by fibrillatory conduction emanating from a small number of high-frequency reentrant sources (rotors). Our goal was to study the ionic correlates of a rotor during simulated chronic AF conditions. We utilized a two-dimensional (2-D), homogeneous, isotropic sheet (5×5 cm^2) of human atrial cells to create a chronic AF substrate, which was able to sustain a stable rotor (dominant frequency ~5.7 Hz, rosette-like tip meander ~2.6 cm). Doubling the magnitude of the inward rectifier K^+ current (I_{K1}) increased rotor frequency (~8.4 Hz), and reduced tip meander (~1.7 cm). This rotor stabilization was due to a shortening of the action potential duration and an enhanced cardiac excitability. The latter was caused by a hyperpolarization of the diastolic membrane potential, which increased the availability of the Na^+ current (I_{Na}). The rotor was terminated by reducing the maximum conductance (by 90%) of the atrial-specific ultrarapid delayed rectifier K^+ current (I_{Kur}), or the transient outward K^+ current (I_{to}), but not the fast or slow delayed rectifier K^+ currents (I_{Kr}/I_{Ks}). Importantly, blockade of I_{Kur}/I_{to} prolonged the atrial action potential at the plateau, but not at the terminal phase of repolarization, which led to random tip meander and wavebreak, resulting in rotor termination. Altering the rectification profile of I_{K1} also slowed down or abolished reentrant activity. In combination, these simulation results provide novel insights into the ionic bases of a sustained rotor in a 2-D chronic AF substrate.

INTRODUCTION

Atrial fibrillation (AF) is the most common form of sustained cardiac arrhythmia in patients, and is the primary cause of stroke (Jalife et al., 1998; Nattel, 2002a). Although non-pharmacological modalities such as catheter ablation and pacing have been developed, their efficacy in the treatment of AF remains limited (Scheinman and Morady, 2001), and pharmacological intervention remains the mainstay of managing AF (Nattel et al., 2002b). However, available drugs also have only modest efficacy for terminating AF and maintaining sinus rhythm (Nattel et al., 2002).

The need for developing more effective antiarrhythmic drugs has intensified efforts aimed at understanding the pathophysiological mechanisms underlying AF. The most widely accepted conceptual model of reentrant activity in AF has been the multiple wavelet hypothesis (Moe, 1962). However, more recent experimental studies suggest that, at least in certain cases, the maintenance of AF may depend upon the periodic activity of one or a small number of sustained, high frequency, functional reentrant sources, i.e., rotors (Jalife et al., 2002; Jalife, 2003). In such a scenario, controlling or terminating the so-called ''mother rotor'' thus represents a valid target for antiarrhythmic drugs. Therefore, understanding the ionic mechanisms that underlie rotor dynamics during AF is of potential significance.

A recent simulation study incorporated the alterations in ionic currents seen during chronic AF (CAF) into a mathematical model of an isolated human atrial cell, and was able to reproduce the experimentally observed shortening of the action potential duration (APD) (Courtemanche et al., 1999). The study also compared the effects of blocking different K^+ currents on repolarization during CAF, and found that blocking a combination of delayed rectifiers ($I_{Kr} + I_{Kur}$) resulted in the maximum prolongation of the APD, leading the authors to suggest that I_{Kur} may be a valuable target for antiarrhythmic therapy (Courtemanche et al., 1999).

However, it is uncertain whether the results obtained at a single-cell level can be extrapolated to the propagation of the electrical impulse in the cardiac muscle, where in addition to the membrane properties, passive properties of the tissue and wavefront curvature play important roles (Cabo et al., 1994, 1996). Furthermore, the above study did not consider the potential effect of changes in the cardiac inward rectifier K^+ current (I_{K1}), which has been found to be upregulated during CAF in humans (Van Wagoner et al., 1997; Bosch et al., 1999; Dobrev et al., 2001). The clinical impact of an increased I_{K1} remains unclear and needs to be addressed (Dobrev and Ravens, 2003), since recent experimental studies suggest that I_{K1} is a major determinant of rotor stabilization and wavefront dynamics during ventricular fibrillation (VF) (Samie et al., 2001; Warren et al., 2003).

Submitted January 31, 2005, and accepted for publication March 10, 2005.

Sandeep V. Pandit and Omer Berenfeld contributed equally to this work.

Address reprint requests to Dr. José Jalife, Institute for Cardiovascular Research and Dept. of Pharmacology, State University of New York Upstate Medical University, Syracuse, NY 13210. Tel.: 315-464-7949; Fax: 315-464-8000; E-mail: jalifej@upstate.edu.

0006-3495/05/06/3806/16 $2.00

doi: 10.1529/biophysj.105.060459

Accordingly, we extended previous single-cell simulation studies in CAF (Courtemanche et al., 1999) by focusing on the dynamics of a single rotor in a two-dimensional (2-D) lattice of cardiac cells. The main goal was to determine the ionic mechanisms that help maintain, or can terminate, a rotor under simulated CAF conditions. We therefore constructed a simplified 2-D model of human atrial cells that was devoid of any structural or electrophysiological heterogeneities, since adding these complexities can confound the interpretation of the ionic mechanisms underlying rotor dynamics (Tung et al., 2004).

The results from our simulation study indicate an important role for I_{K1} in stabilizing rotors during CAF. Additionally, they show that specific blockade of the ultrarapid delayed rectifier K^+ current, I_{Kur}, or the transient outward K^+ current, I_{to}, (but not the fast or slow delayed rectifiers, I_{Kr} or I_{Ks}, respectively) can terminate rotor activity.

METHODS

Single-cell simulations

A mathematical model of the human atrial myocyte (Courtemanche et al., 1998) was implemented in ''C'' language, on a SUN Ultra-10 workstation platform. The differential equations in this model were solved using a fixed-time-step ($\Delta t = 0.005$ ms), modified Euler method, as in an earlier study (Courtemanche et al., 1998). The CAF conditions were simulated by incorporating changes in the model parameters in accordance with an earlier study (Courtemanche et al., 1999). Two CAF conditions were simulated:

The CAF1 case

This was simulated by incorporating a downregulation in the densities of the transient outward K^+ current, I_{to} (by 50%), the ultrarapid delayed rectifier K^+ current, I_{Kur} (by 50%), and the L-type Ca^{2+} current, I_{CaL} (by 70%), as in an earlier study (Courtemanche et al., 1999).

The CAF2 case

The changes were similar to the CAF1 case. However, an additional increase in the density of the inward rectifier K^+ current, I_{K1} (by 100%), was also incorporated. This was based on experimental data, which showed that the magnitude of I_{K1} was almost doubled in left atrial myocytes isolated from patients in chronic AF (Van Wagoner et al., 1997).

The steady-state cardiac action potentials in CAF1 and CAF2 were obtained by pacing the ionic model for 13 s at 1 Hz (after making the respective parameter changes). These action potentials were then incorporated into the 2-D sheet, which was used to simulate spiral-wave activity.

To assess the contribution of an ionic current to the APD, we reduced the maximum conductance value of the ionic current of interest by 90%, except for I_{K1} and $I_{Ca\text{-}L}$, in accordance with earlier studies (Courtemanche et al., 1999). $I_{Ca\text{-}L}$ was reduced by 75% to mimic the effect of verapamil in accordance with an earlier study (Samie et al., 2000), and the I_{K1} current density was reduced by 20%, since further reduction leads to model instability and disruption of normal repolarization (Courtemanche et al., 1999).

2-D simulations

The propagation of the cardiac impulse was simulated in a two-dimensional (2-D), homogeneous, isotropic tissue of area 5×5 cm^2, consisting of 500×500 nodes (atrial cells), and no-flux boundary conditions at the edges. We used the Euler method to integrate the voltage at each node, which was governed by the conventional reaction-diffusion equation, assuming uniform, isotropic tissue:

$$\frac{\partial V}{\partial t} = -\frac{I_{ion}}{C_m} + D\left(\frac{\partial^2 V}{\partial x^2} + \frac{\partial^2 V}{\partial y^2}\right),$$

where V is the membrane voltage, I_{ion} is the total membrane ionic current, C_m is the membrane capacitance, and D is the diffusion coefficient. The time step for integration was 0.01 ms, the space step was 0.1 mm, C_m was 100 pF, and the value of D was 0.1 mm^2/ms. The 2-D simulations were coded in ''C'', and solved on a 32 processor, parallel computer (MicroArray cluster machine). Rotors were initiated by the standard cross-field stimulation protocol (separately for the CAF1 and CAF2 conditions), and the reentrant activity studied for a duration of 10 s, which required $\approx$40 h of run time on the parallel computer. Since the internal ionic concentrations in the human atrial cell model have not been balanced for long-term simulations, $[Na^+]_i$ and $[K^+]_i$ were not allowed to vary with time, as in an earlier study (Xie et al., 2002). We also simulated the effects of blocking various ionic currents on spiral-wave activity in the CAF1 condition. The spiral was allowed to run in the CAF1 condition for 1 s initially, and then the maximum conductance values of the ionic currents were reduced, as described previously in single-cell simulations.

Analysis of spiral waves

We analyzed the behavior of the spiral waves obtained in the 2-D simulations by calculating pseudoelectrocardiograms (pseudo-ECGs) and power spectral densities, as well as examining phase movies. Part of the analysis was done using the MATLAB software package, which was used to calculate the pseudo-ECG by integrating the spiral-wave signal over the entire 2-D sheet, analogous to an earlier study (Skanes et al., 1998). This pseudo-ECG was then used to calculate the power spectral density (using the ''psd'' function available in MATLAB), which allowed us to obtain the maximum dominant frequency (DF). For obtaining a measure of the spiral-wave tip trajectory, we first constructed a phase movie as in earlier studies (Gray et al., 1998). Briefly, the instantaneous phase at each node was determined by plotting the value of the transmembrane voltage at time t ($F(t)$), against the value of the transmembrane voltage at the same node offset by a time interval τ, where τ = one-quarter of the period of the dominant frequency of the spiral wave ($\approx$5 Hz in our simulations, as can be seen in Results). A cyclic return map of $F(t)$ versus $F(t - \tau)$ was constructed, and the phase was defined as the angle of the coordinate $[F(t), F(t - \tau)]$ around the mean signal for that given node, with values between $-\pi$ and π represented as a continuous color scheme from red to purple. The phase singularity (PS) was defined as a point where all phases converged, and can also be thought of as the point of intersection where the depolarizing front and repolarizing tail of a reentrant wavefront meet (Jalife, 2000). The phase movie was utilized to track the PS manually, and the maximum tip meander in the x and y directions in the 2-D sheet was averaged to estimate the spiral-tip meander.

RESULTS

Simulated action potentials and spiral waves in chronic AF

Fig. 1 *A* displays the simulated action potentials in single cells under control and chronic AF conditions; the APD was abbreviated in CAF1, and more so in CAF2. An increase in I_{K1} (CAF2) also caused a small hyperpolarization of the resting membrane potential (V_{rest}) by $\sim$3.3 mV compared to control. This is in accordance with recent experimental

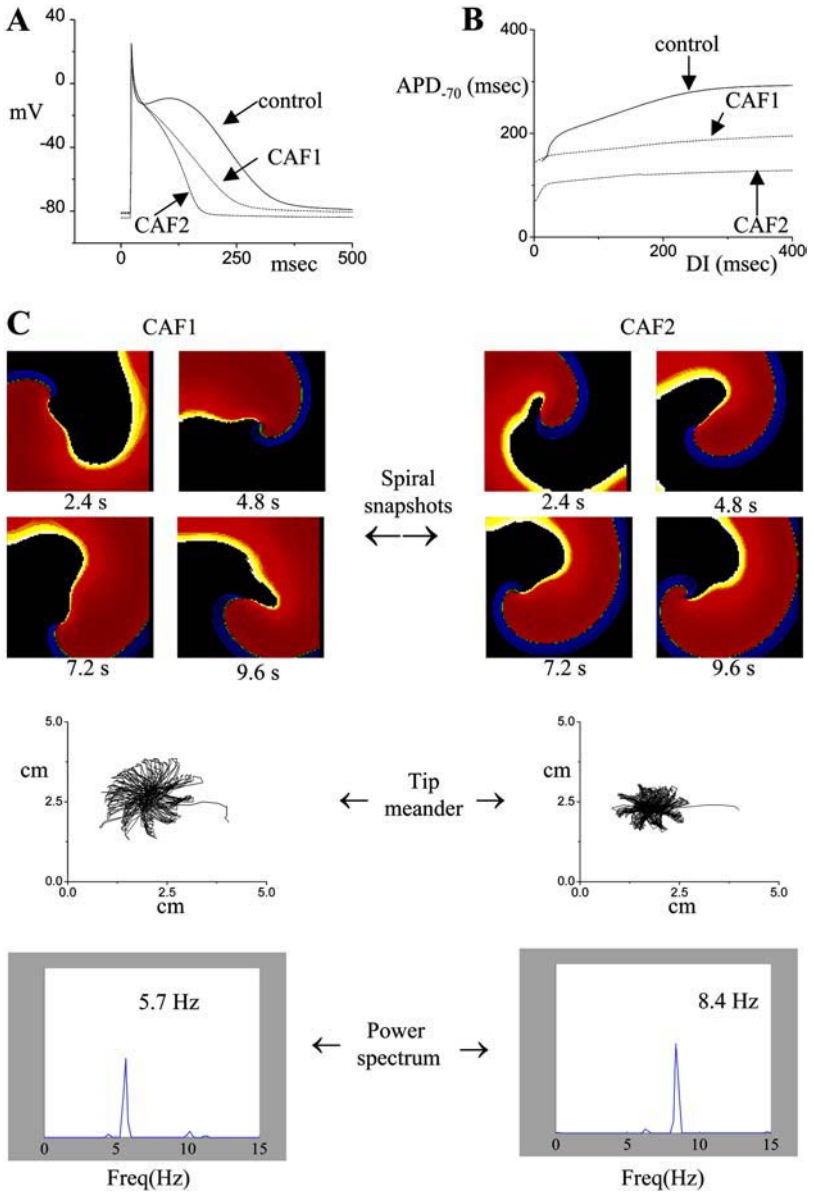

FIGURE 1 (*A*) Simulated action potentials in control and chronic AF conditions (*CAF1*, *CAF2*). (*B*) Electrical restitution plotted as APD_{-70} versus the diastolic interval (*DI*) in control and chronic AF cases. (*C*) Spiral waves (phase movie snapshots), tip meander, and power spectral densities in chronic AF conditions CAF1 and CAF2. Phase movies are shown at four distinct times (2.4, 4.8, 7.2, and 9.6 s). The tip meander is plotted in a 5×5 cm^2, 2-D atrial sheet.

results, which showed that the mean V_{rest} was hyperpolarized by 3.6 mV in chronic AF conditions when I_{K1} was increased (Dobrev et al., 2001). Fig. 1 *B* displays the steady-state electrical restitution curves, where the APD at -70 mV was plotted versus the diastolic interval (*DI*), in accordance with a previous study (Xie et al., 2002). The restitution curve is flatter in chronic AF conditions compared to control, and the curves for the CAF1 and control cases tend to converge at short DIs, as observed experimentally in humans (Franz et al., 1997). The slope of the restitution curve is >1 only at very small DI values in chronic AF. Experimental results regarding electrical restitution obtained from chronic AF patients remain controversial, and slopes either <1 (Franz et al., 1997) or >1 (Kim et al., 2002) have been reported.

A sustained rotor was inducible when the APD was shortened in chronic AF, but not in healthy conditions. Fig. 1 *C* shows representative snapshots of phase movies of spirals in both the CAF1 and CAF2 conditions, at time intervals of 2.4 s. The spiral tip displayed a quasiperiodic meander with a rosette-like pattern in both the CAF1 and CAF2 cases (Fig. 1 *C*). The tip meander was ~2.6 cm in CAF1, and ~1.7 cm in CAF2. Pseudo-ECGs of the spiral waves (not shown) were analyzed to calculate power spectral densities; the DF in the CAF2 case (~8.4 Hz) was greater than that in the CAF1 case (~5.7 Hz).

Mechanisms of rotor stabilization in CAF2

Since Na^+ current (I_{Na}) primarily determines the speed of wavefront propagation, we investigated its behavior in CAF conditions during reentry. The top panels in Fig. 2 *A* depict the distribution of the transmembrane voltage in the CAF1

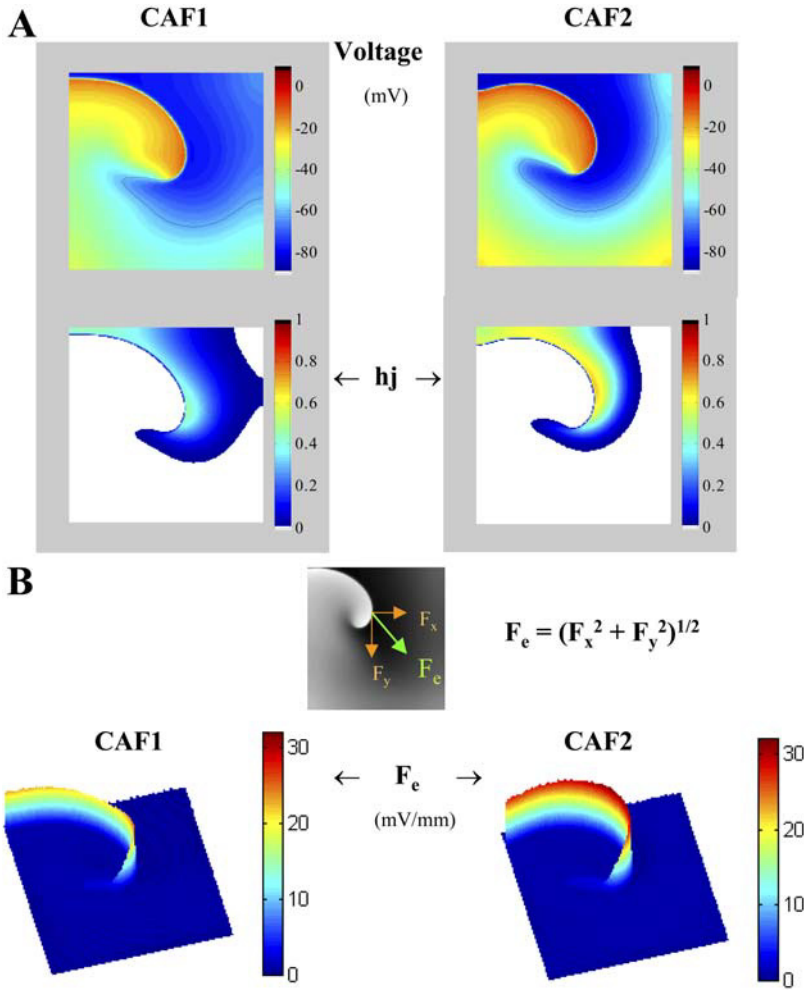

FIGURE 2 (*A*) Plot of the transmembrane voltages and the underlying ''product'' of the inactivation variables of I_{Na} (***hj***) in CAF1 and CAF2, at $t = 4.04$ s. The panels contain a contour line (*black*) representing the transmembrane voltage at –60 mV. (*B*) Top panel contains the schematic of the electrotonic current (F_e) at each node (cell) in the 2-D sheet, and is computed from F_x and F_y (voltage gradients in the *x* and *y* directions). Bottom panels show a 3-D representation of F_e (mV/mm) in the CAF1 and CAF2 conditions.

(*left*) and CAF2 (*right*) conditions, at $t = 4.04$ s. The maximum/minimum values of the membrane voltages in CAF1 and CAF2 were $-10.0/-78.4$ mV and $-5.2/-83.2$ mV, respectively. Also superimposed in each of the top panels is a black curve at -60 mV, which separates the inexcitable portion of the cycle, or wavelength (positive to -60 mV), and excitable tissue (the excitable gap, negative to –60 mV; the *dark blue region*). A more direct measure of the excitable gap can be obtained by studying the distribution of ***hj*** (the product of the fast, ***h***, and the slow, ***j***, inactivation variables of I_{Na}) as shown in the panels below the voltage distribution in Fig. 2 *A*. The maximum value of ***hj*** was 0.692 in CAF2, compared with 0.468 in CAF1. Thus, the excitable gap (represented by the colored area in the panels for ***hj***) allowed ''more recovery'' in the CAF2 case (*yellow region* in Fig. 2 *A* for ***hj***), resulting in a higher magnitude of I_{Na} (-17.6 nA in CAF2 compared to -12.0 nA in CAF1), and therefore a faster rotation frequency.

An increase in I_{Na} should cause a corresponding increase in the electrotonic depolarizing current at the wavefront, which is important because it will then allow the wavefront to overcome the increased current requirements for excitation due to the higher I_{K1} density in CAF2. A measure of the electrotonic current (F_e) at each node (or cell) in the 2-D sheet in a given spiral-wave snapshot was obtained by first calculating the voltage gradients in the *x* (F_x) and the *y* (F_y) directions, and then estimating the magnitude of $F_e = (F_x^2+F_y^2)^{1/2}$, as depicted schematically in the top panel in Fig. 2 *B*. The plots of the three-dimensional (3-D) map of F_e (mV/mm) in the CAF1 and CAF2 conditions (at $t = 4.04$ s) are shown in the bottom panels in Fig. 2 *B*. In both the CAF1 and CAF2 cases, the electrotonic current is seen to be the largest along the depolarizing wavefront, and is also greater in CAF2 compared to CAF1.

We further investigated the cause for an increase in the availability of I_{Na} in CAF2 at the cellular level. We began by pacing the atrial model at a basic frequency just below the DF in AF: 5 Hz for CAF1 and 8 Hz for CAF2. The values of ***hj*** underlying the membrane potential are plotted in Fig. 3 *A*. The value of ***hj*** is larger for CAF2, despite the higher frequency (8 Hz), which initially seems counterintuitive. To determine why ***hj*** is larger for CAF2, we studied the behavior of ***hj*** variables under voltage-clamp conditions as shown in Fig. 3 *B*. The top panels show the triangular,

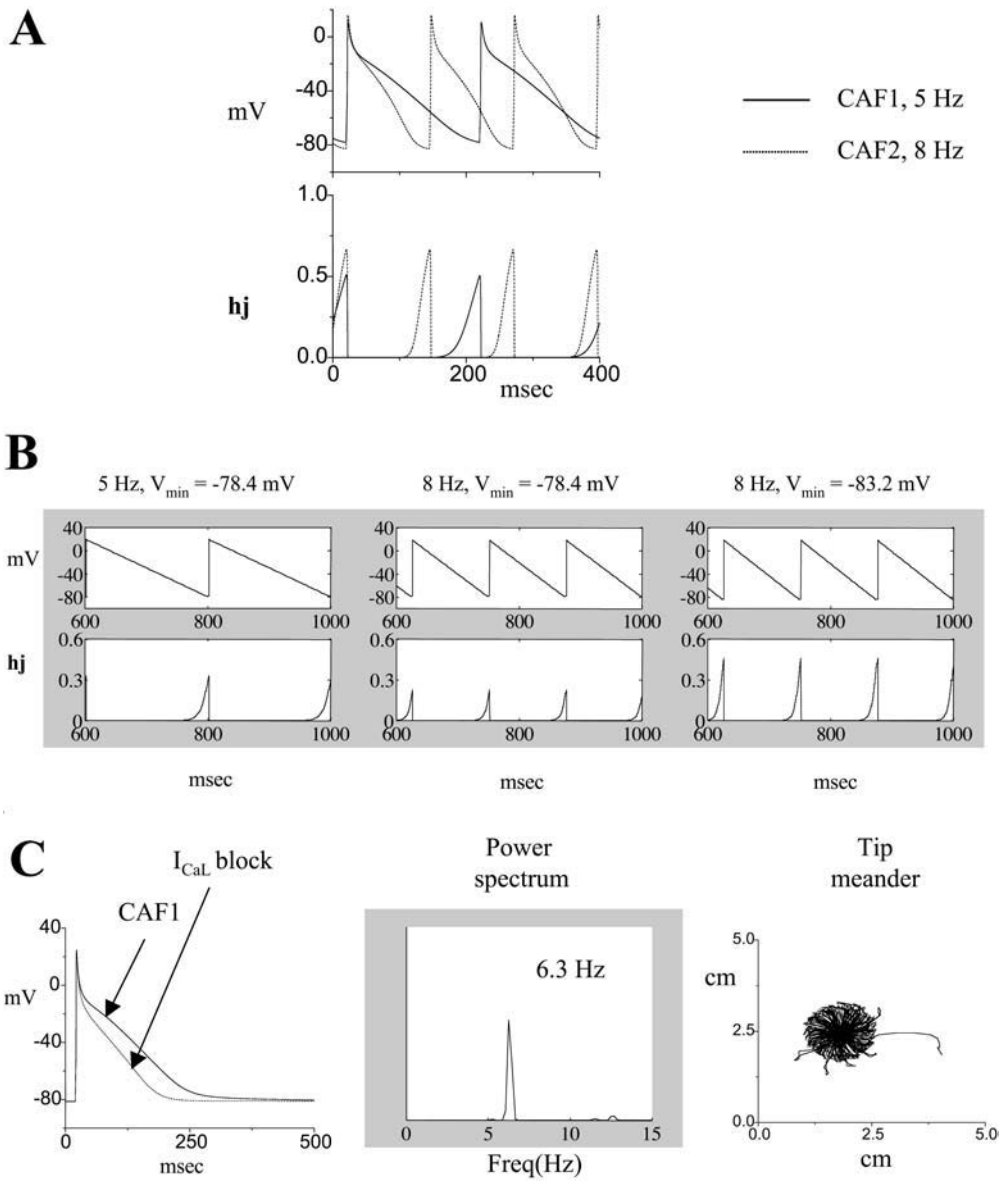

FIGURE 3 (*A*) Simulated action potentials and underlying ***hj*** in single-cell atrial models paced at 5 Hz and 8 Hz in the CAF1 and CAF2 conditions, respectively. (*B*) Descending voltage-clamp ramps (from +20 mV to either –78.4 or –83.2 mV) at either 5 Hz or 8 Hz, and the underlying values of ***hj***. (*C*) Simulated action potential in the CAF1 condition when $I_{Ca\text{-}L}$ was blocked (by 75%), and the corresponding power spectral density and tip meander of the rotor.

generic action potential clamp protocol used to assess aspects of Na^+-channel function under CAF conditions. In the first case (*left panel*), ***hj*** was clamped to a series of descending ramps from +20 mV to −78.4 mV at a frequency of 5 Hz (−78.4 mV is the most negative diastolic potential of the CAF1 case). The clamp included a 2-ms plateau at the most negative diastolic potential to mimic the initial depolarization phase of the action potential. Increasing the frequency to 8 Hz, but with a similar diastolic value of −78.4 mV (*center*) decreased the maximum value of ***hj***; however, when the diastolic potential was clamped to −83.2 mV as seen in CAF2 (*right*), ***hj*** was increased, and was now even higher than that obtained at 5 Hz (*1left*). Thus, in the Courtemanche model, the key factor responsible for the increased availability of I_{Na} in CAF2 is the hyperpolarization of the diastolic membrane voltage by ~5 mV, which results in a faster recovery of I_{Na}.

An increased I_{K1} also leads to a shortening of the APD in CAF2. To assess the effects of a shortened APD on rotor dynamics independent of the hyperpolarization in V_{rest}, we simulated conditions for reduction of $I_{Ca\text{-}L}$ (by 75%), as in an earlier study (Samie et al., 2000). The resultant shortening of the APD and the corresponding rotor characteristics are shown in Fig. 3 *C*. Interestingly, the rotor again accelerated (DF ~6.3 Hz) compared to CAF1 (~5.7 Hz), but this acceleration was less compared to that observed in CAF2 (~8.4 Hz). In contrast, the spiral-tip meander was reduced (~2.0 cm), compared to CAF1 (~2.6 cm). These results reemphasize the fact that in addition to a shortening of the APD (which occurs when either I_{K1} is increased or $I_{Ca\text{-}L}$ is

blocked), increased availability of I_{Na} is an important factor in mediating rotor acceleration when I_{K1} is increased, due to hyperpolarization of diastolic membrane potential (which does not occur when $I_{Ca\text{-}L}$ is blocked). Additionally, these results also show that $I_{Ca\text{-}L}$ is an important determinant of spiral-tip meander in this ionic model. Experimental results regarding Ca^{2+} current blockade in AF are controversial; one study reported a reduced fibrillatory frequency when patients were treated with oral verapamil (Bollmann et al., 2002), whereas others indicated that verapamil shortened AF cycle length (Sticherling et al., 2002). The latter experimental results are in accordance with our simulation results. Additionally, an earlier study utilizing the Luo-Rudy ventricular model showed that $I_{Ca\text{-}L}$ block reduced the frequency of rotors by increasing their core size (Samie et al., 2000), which seems contradictory to our results. The reasons for this discrepancy are not clear, and other than the ionic differences between the atrial and ventricular models, could also be related to the fact that in our simulations using an atrial model, quasiperiodic meandering rotors are observed, whereas in the previous study, stable rotors with a stationary core area were observed (Samie et al., 2000). We were unable to induce a rotor with a stationary circular core using the Courtemanche atrial model.

Effect of reducing K^+ currents on rotor dynamics

We next analyzed the effect of reducing the maximum conductance values of different K^+ currents (excluding I_{K1}) on rotor dynamics in the CAF1 condition. We did not seek to model or mimic the actions of any antiarrhythmic drug, because Hodgkin-Huxley type models (such as those utilized in this study) are limited in their ability to simulate the ''state-dependent'' effects of drugs (Liu and Rasmusson, 1997), and such effects are best simulated by employing markovian models of K^+ channels (Campbell et al., 1993a,b). Instead, the objective was to utilize the Courtemanche atrial model as a tool to assess the contribution of different K^+ channels to spiral-wave behavior in a simple yet effective way, and identify potential targets amongst the available ionic milieu for antiarrhythmic therapy. A similar approach has previously provided valuable insights into the contribution of different ionic current(s) to the cardiac action potential (Courtemanche et al., 1999; Wettwer et al., 2004) and/or rotor dynamics in 2-D simulations (Samie et al., 2000; Xie et al., 2002). The rotor characteristics (pseudo-ECG, dominant frequency, and tip meander), analyzed for 9 s (or until the rotor terminated) during blockade of each specific ionic current after allowing the rotor to run in the CAF1 condition for 1 s, are compared in Fig. 4. The rotor terminated when either I_{Kur} or I_{to} was suppressed, but not during I_{Kr} or I_{Ks} blockade. Analyzing the spectral densities during current blockade showed that the maximum frequencies were slightly reduced in all the cases, compared to the DF in CAF1 ($\sim$5.7 Hz). Interestingly, the tip meander maintained a rosette-like pattern during either I_{Kr} or I_{Ks} blockade, but was considerably disorganized when I_{Kur} or I_{to} was suppressed.

The rotor termination is shown in Fig. 5 for (*A*) I_{Kur} block, and (*B*) I_{to} block. An initial breakup of the spiral wavefront in each case is seen to occur at a line of conduction block (depicted by a *white line* at $t = 3.44$ s in panel *A* and at $t = 5.49$ s in panel *B*), and away from the spiral tip. In the case of I_{Kur} block, the breakup resulted in two wavelets, which merged almost immediately, but the resulting wavefront could not sustain its reentrant behavior and terminated subsequently. The breakup during I_{to} blockade led to only one of the wavelets rotating for two more cycles, before its final termination.

Mechanism(s) for rotor tip meander and wavebreak

A rigorous, quantitative analysis of rotor tip meander is extremely complex for ionic models (Courtemanche, 1996; Fenton et al., 2002); hence, we have attempted to achieve a qualitative understanding of the observed differences in spiral-tip meander and reentry termination during ionic current blockade. In Fig. 6 *A*, we compare the distribution of the transmembrane voltage in the 2-D sheet during I_{Kr} and I_{Kur} blockade. The dashed and solid lines in the voltage maps represent isopotentials at -15 mV (approximately representing the plateau and pointed to be the *black arrows*) and -60 mV (approximately representing the wavetail), respectively. In the case of I_{Kur} block, there was an elevation of the plateau potential at $t = 2.51$ s, which resulted in a ''kink'' (*upper left quadrant*) that delayed repolarization and therefore slowed the clockwise propagation of the wavetail. Comparison of equivalent times of propagation in the I_{Kr} block and I_{Kur} block cases (see *red arrows*) reveals that the wavetail indeed propagates more slowly in the latter, even though the wavefronts are similar in both (which can also be surmised by the different rotor frequencies in Fig. 4). This results in more complex wavefront-wavetail interactions, and plausibly underlies the disorganized tip meander pattern seen in I_{Kur} block (Fig. 4 *C*). The actual occurrence of a wavebreak during I_{Kur} blockade is shown in Fig. 6 *B*, which depicts the membrane voltage (*upper snapshots*) and the underlying ***hj*** variables (*lower snapshots*). Here, the previous formation of the ''kink'' sets the stage for a portion of the depolarizing wavefront encountering insufficiently recovered tissue ($t = 3.40$ s). Consequently, the wave front breaks up into two distinct wavelets, which later collide, fuse, and propagate toward the upper border of the sheet (see Fig. 5). In the meantime, the original meandering spiral tip runs into the right border ($t = 3.48$ s), terminating the rotor activity.

In Fig. 7, we present additional simulation results regarding rotor characteristics during I_{Kr} and I_{Kur} blockades, respectively. We quantified the area occupied by the plateau

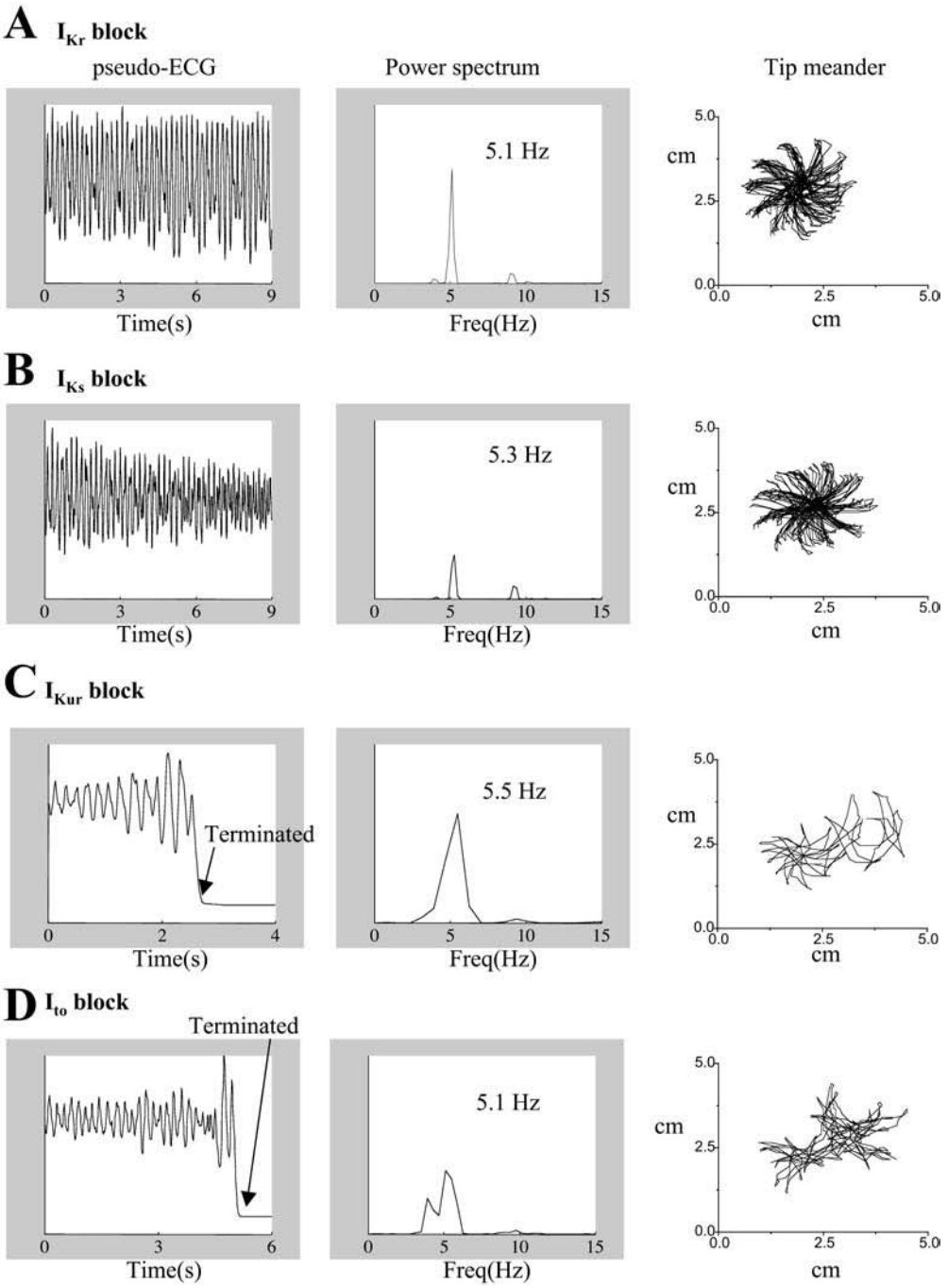

FIGURE 4 Rotor characteristics, including pseudo-ECGs, power spectral densities, and spiral-tip meander during (*A*) I_{Kr} block, (*B*) I_{Ks} block, (*C*) I_{Kur} block, and (*D*) I_{to} block.

phase of the action potential (approximately represented by the transmembrane voltage which lies between 5 and −20 mV) as a percentage of the total area of the 5×5 cm^2 human atrial 2-D sheet (Fig. 7 *A*). This area was quantified between 1 and 4 s (since the block of ionic currents was started after allowing the rotor to run for 1 s in the CAF1 condition, and I_{Kur} terminated after ≈3.5 s). The percent area was sampled at 10-ms intervals, and was seen to 1), vary with time, and 2), be larger during I_{Kur} block (*red*), compared to I_{Kr} block (*black*). The presence of these larger kinks during I_{Kur} block prevented the rotor tip from pivoting sharply, and pushed it toward the sheet boundary. This is seen in Fig. 7 *B*, where we have plotted the positions of the spiral tip during I_{Kr} and I_{Kur} current blockades (sampled every 10 ms) in the 2-D atrial sheet for a time between 1 and 4 s (Fig. 7 *B*). This plot shows that the rotor is near the sheet boundary more times during I_{Kur}, compared to I_{Kr} block.

In summary, these results suggest that the I_{Kur} blockade elevates the plateau potential, resulting in a slower wavetail whose interaction with the spiral tip produces 1), chaotic tip

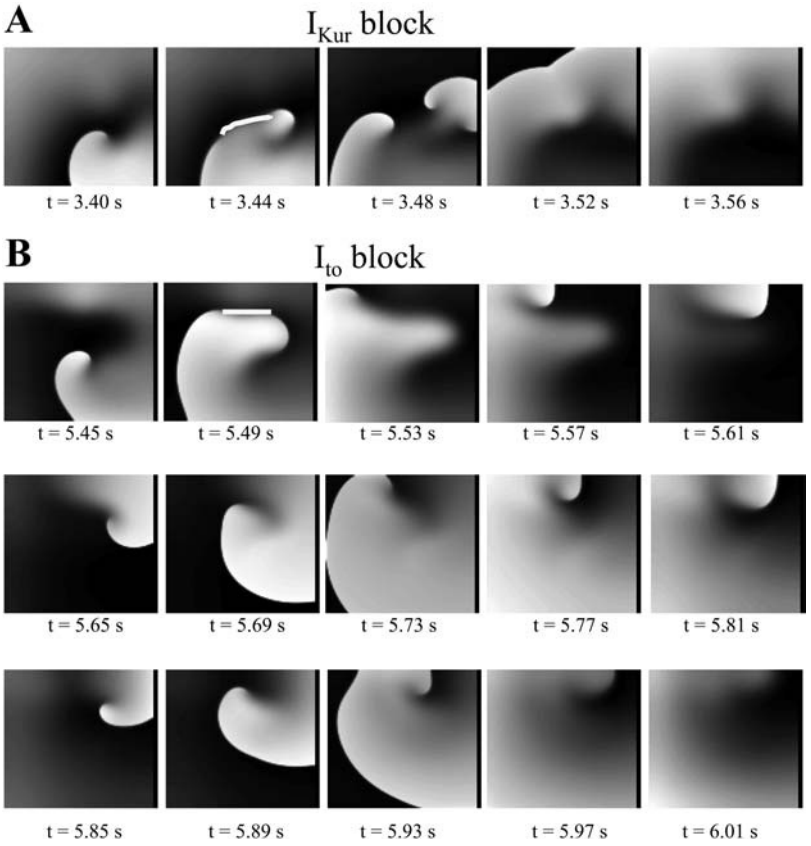

FIGURE 5 Snapshots of spiral wave in the CAF1 condition demonstrating instances of wavebreak during blockade of (*A*) I_{Kur}, and (*B*) I_{to}. The white line in the snapshots (at $t = 3.44$ s in panel *A* and $t = 5.49$ s in panel *B*) schematically depicts the occurrence of a conduction block along the wavefront just before wavebreak.

meander, and 2), a wavebreak, creating conditions conducive for rotor termination by collision of the tip with a boundary.

Can cellular APD act as a predictor of rotor termination?

We also investigated the effects of specific K^+ channel blockade on the plateau and final phases of repolarization at the single-cell level, to determine whether there was a correlation between prolongation at the action potential plateau per se and rotor termination. Fig. 8 *A* displays representative APDs when I_{Kr} and I_{Kur} were blocked in the CAF1 case (at 1 Hz). The terminal phase of repolarization is longer during I_{Kr} than I_{Kur} block; in contrast, the plateau was more prolonged during I_{Kur} block. The elevated plateau phase during I_{Kur} block was also associated with a slower inactivation of the underlying $I_{Ca\text{-}L}$, compared to I_{Kr} block (Fig. 8 *B*). Interestingly, a similar preferential prolongation of the plateau potentials by I_{Kur} block (in the presence of low concentrations of 4-aminopyridine, a selective blocker of I_{Kur}) has also been observed experimentally recently in action potentials recorded in right atrial appendages isolated from chronic AF patients (Wettwer et al., 2004).

The action potentials in a single cell (at 1 Hz, CAF1 case) during blockade of the different K^+ currents are depicted in Fig. 9 *A*. The action potentials depicted by dashed lines represent cases in which the rotor was terminated. The APD was more prolonged at -15 mV during I_{to} and I_{Kur} blockade than during all other cases. (However, in contrast, $I_{Kr} + I_{Ks}$ blockade showed the largest prolongation at -70 mV, and is discussed in greater detail in the next section). Fig. 9 *B* summarizes the prolongation in the APD at -15 mV and at -70 mV (representing the terminal phase of repolarization) during specific ionic current blockades, compared to control (the CAF1 case). Rotor termination was indeed related to a maximal prolongation of the APD at the plateau (exception: $I_{Kr} + I_{Ks}$ blockade), rather than a prolongation at the terminal phase of repolarization (the *T* in Fig. 9 *B* indicates cases in which the rotor was terminated).

The steady-state cellular APD restitution curves (at -70 mV, and at 1 Hz) are plotted against the various diastolic intervals (DI) during the CAF1 case, and during the various ionic current blockades (Fig. 10 A). There was no obvious correlation between the slope of the restitution curve and rotor termination (I_{to}, I_{Kur}, and $I_{Kr} + I_{Ks}$ blockades).

$I_{Kr} + I_{Ks}$ blockade

Since individual blockade of I_{Kr} and I_{Ks} currents failed to terminate the rotor, we studied their combined block, and the corresponding rotor characteristics are depicted in Fig. 10 *B*. The rotor terminated during this blockade at ≈5.4 s after the

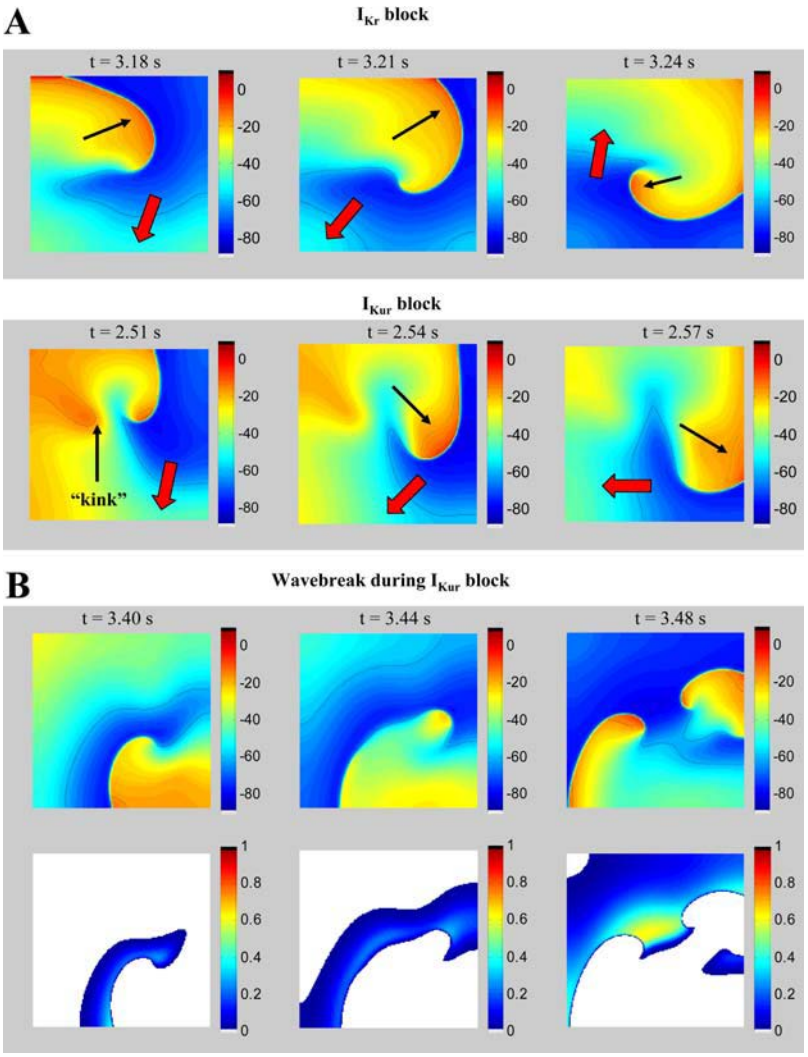

FIGURE 6 (*A*) Snapshots of membrane voltage during rotation of the spiral in I_{Kr} and I_{Kur} blockade. Solid and dashed lines in the voltage panels represent isopotentials at –60 and –15 mV, respectively. The red arrows schematically represent the direction of propagation of the wavetail, and the black arrows point to the –15 mV isopotential line that follows the excitation wavefront. (*B*) Snapshots of membrane voltage and the underlying ***hj*** (excitable gap) during occurrence of wavebreak in I_{Kur} blockade are shown.

block. The dominant frequency (4.1 Hz) was reduced, compared to the CAF1 case (5.7 Hz). The tip meander pattern was considerably disorganized, compared to the CAF1 case. Thus, rotor termination was also possible if the APD prolongation at the terminal phase of repolarization exceeded some critical level. This mechanism plausibly underlies rotor termination during combined I_{Kr} + I_{Ks} blockade, since 1), the prolongation at −70 mV in this case is the largest amongst all blockades studied (Fig. 9 *B*), and the prolongation at −15 mV is also smaller than that during I_{Kr} blockade (when the rotor did not terminate); and 2), the rotor termination during combined I_{Kr} + I_{Ks} block did not involve a wavebreak, as was seen during I_{to}/I_{Kur} block (see movie in Supplementary Material).

Alterations in the inward rectifier, I_{K1}

Since an increase in I_{K1} accelerated the spiral, it was logical to ask whether specific blockade of I_{K1} current could abolish it. Suppressing the maximum conductance of I_{K1} (by 20%) slowed, but did not terminate, the rotor. As an alternative, we therefore studied the effects of altering the rectification profile of I_{K1}. The top and middle panels in Fig. 11 show different rectification profiles of I_{K1} and their corresponding effect on the action potential waveforms. In panel *A*, the equation of I_{K1} was modified such that the magnitude of the peak outward component of that current decreased gradually, from 51.5 pA in case 1, to 40 pA in case 2, and to 27 pA in case 3. However, the current rectified completely (<1 pA) at very depolarized potentials (18 mV for case 1, and 27 mV for cases 2 and 3, respectively). This resulted in a progressive but slight prolongation of the APD, but an appreciable depolarization of V_{rest}. As shown in the bottom panel of Fig. 11 *A*, in 2-D spiral-wave simulations, these changes either slowed (case 2) or terminated (case 3) spiral-wave activity. The simulations in panel *B* were in contrast to panel *A*. Here, the equation of I_{K1} was modified such that the magnitudes of the peak outward component were similar (51.5 pA in case 1, 50 pA in case 2, and 47 pA in case 3); however, the outward I_{K1} rectified completely (<1 pA) at progressively more

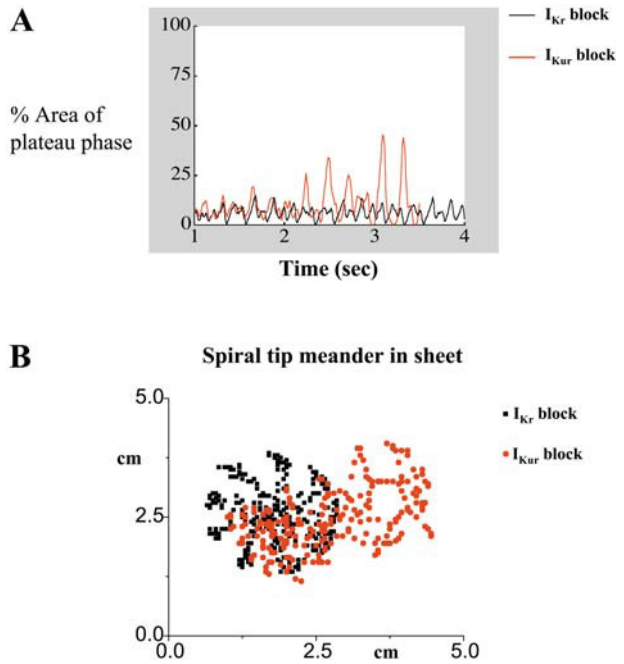

FIGURE 7 (*A*) Plot of the percent area of the 5 × 5 cm^2 human atrial sheet, where the transmembrane voltage lies between 5 and –20 mV (≈ representing the plateau phase) for both I_{Kr} block (*black*) and I_{Kur} block (*red*), for a time between 1 and 4 s (when the currents were blocked). (*B*) Plot of the spiral-tip position during I_{Kr} block (*black squares*), and I_{Kur} block (*red dots*), sampled every 10 ms in the 2-D atrial sheet for a time period of the respective rotors between 1 and 4 s.

hyperpolarized potentials, i.e., at 18 mV, −13 mV, and −37 mV in cases 1, 2, and 3, respectively. These changes in I_{K1} had a more pronounced effect on the APD than on V_{rest}, which in 2-D simulations resulted in a reduction of the spiral-wave frequency, and eventual termination (*bottom panel*).

DISCUSSION

The two main findings of our simulation study are:

1. Upregulation of I_{K1} accelerates and stabilizes rotor activity in CAF. This finding is consistent with earlier studies from our laboratory, which have suggested an important role for I_{K1} in sustaining rotor dynamics during VF (Samie et al., 2001). But in addition to confirming a similar role for I_{K1} in the atrium, our simulations clearly show for the first time the mechanisms that are involved in rotor stabilization in CAF: APD shortening and an increased availability of I_{Na} are major factors that control rotor acceleration, and $I_{Ca\text{-}L}$ is seen to influence tip meander.
2. Individual blockade of I_{Kur} or I_{to} (but not I_{Kr} or I_{Ks}) causes rotor termination; the simulations demonstrate that the underlying mechanism is related to a prolongation of the plateau phase (rather than the terminal phase) of the action potential. This induces tip meander and wave-break, ultimately leading to rotor termination. Taken together, these results provide novel mechanistic insights into the ionic bases of functional reentry during simulated CAF conditions in a 2-D model of human atrial cells.

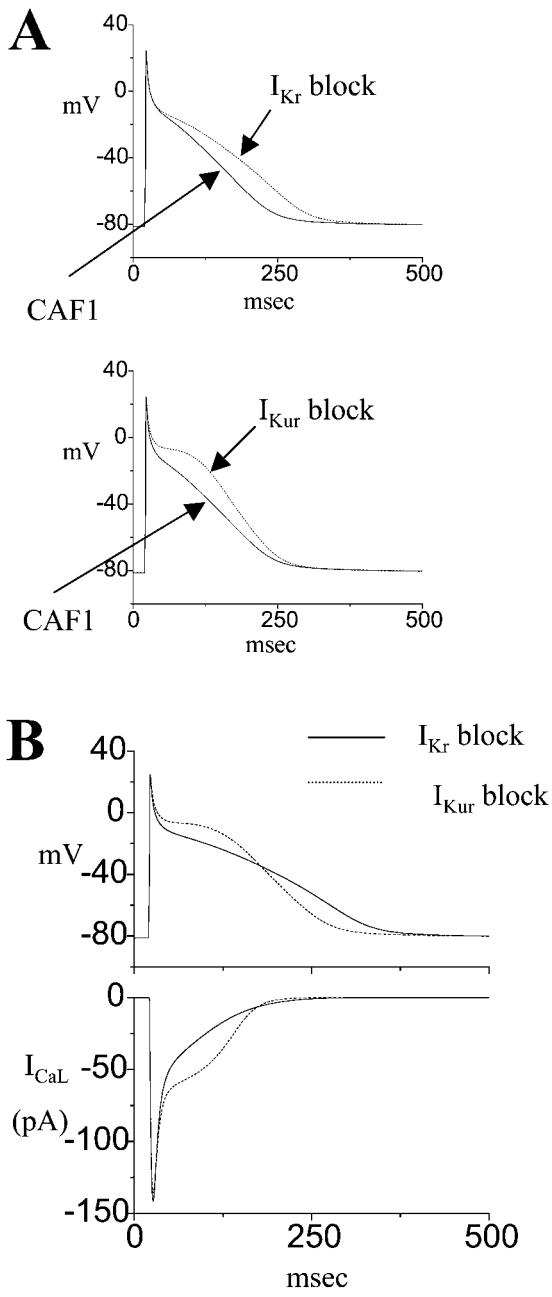

FIGURE 8 (*A*) Representative APDs in the CAF1 condition when I_{Kr} and I_{Kur} were blocked (at 1 Hz), and (*B*) their respective underlying $I_{Ca\text{-}L}$ currents.

Our simulation results must be extrapolated with caution to the in situ atria due to the inherent complexity associated with the latter, and because the results from this study are more applicable to the case where CAF is postulated to be maintained due to a mother rotor, rather than ectopic foci or

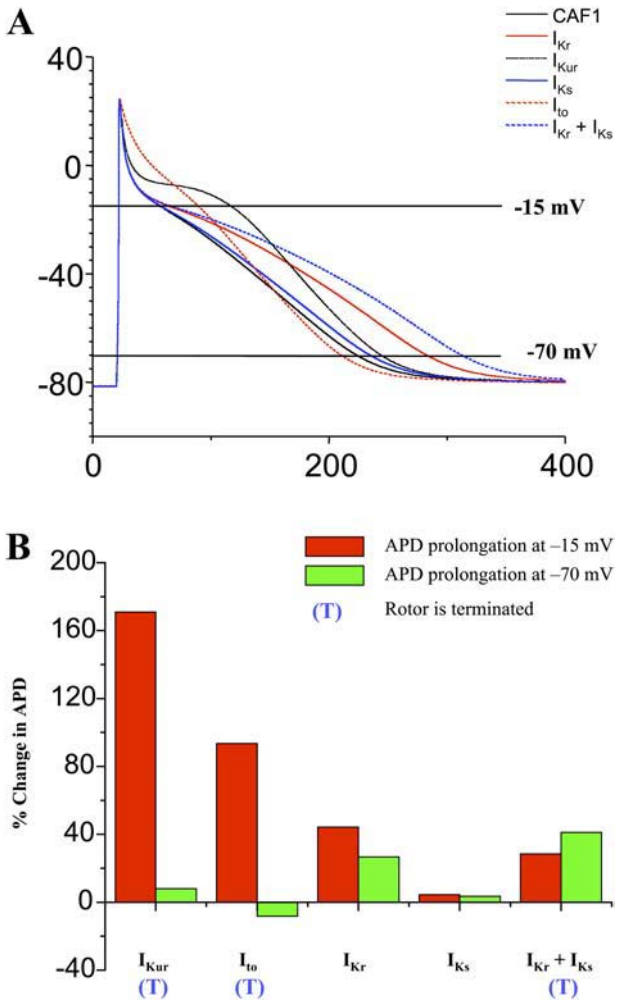

FIGURE 9 (*A*) Steady-state action potentials obtained at the cellular level (1 Hz, CAF1 condition) during various ionic current blockades. The dashed lines represent cases when the rotor was terminated. (*B*) Percentage of prolongation of the APD in a single cell at –15 mV (representing the plateau phase) and at −70 mV (representing the terminal phase of repolarization), during different ionic current blockades, compared to the CAF1 condition (at 1 Hz). The ionic current that is blocked is indicated at the *x* axis, and *T* indicates that rotor termination occurred during this ionic current blockade.

multiple wavelets (Jalife et al., 2002; Jalife, 2003). In subsequent sections of this article, we utilize insights obtained from our simulation results regarding the maintenance and/or termination of the rotor, and compare them to some clinical/experimental observations. Additionally, we address the feasibility of I_{K1} as an antiarrhythmic target, and finally discuss the potential limitations and future extensions of our modeling study.

Sustained rotors in chronic AF

Experimental studies that have mapped the electrical activity of the atria during chronic AF in humans have so far documented the presence of either a focal source of activation, or multiple random wavelets (de Groot and Allessie, 2001). Our simulations demonstrate that it is possible to sustain stable rotors in an electrically remodeled substrate. The simulated rotor frequencies (5.7 Hz and 8.4 Hz in CAF1 and CAF2, respectively, in the Courtemanche et al. model) are within the range of repetitive activation cycle lengths recorded in the left atrium of chronic AF patients, where the cycle lengths varied from 118 ms to 210 ms, or from ~4.8 Hz to 8.5 Hz (Harada et al., 2000). The source of this high frequency activation, i.e., foci or rotors, remains unclear, however. The clinical electrophysiology studies from this same group also suggest that the left atrium (LA) acts as an electrical driving chamber during chronic AF (Harada et al., 2000). Additionally, a very recent study also shows that the patterns of the atrial electrograms in chronic AF patients were consistent with the possibility of a main reentrant source (driver), which was localized for the most part in the left atrium (Sahadevan et al., 2004). At least one study has demonstrated that I_{K1} is increased only in left (not right) atrial myocytes from chronic AF patients (Van Wagoner et al., 1997). Our simulations show that a larger I_{K1} can induce a faster spiral rotation, and thus may provide a partial explanation for the localization of the fastest reentrant source in the LA during AF (Jalife, 2003).

Normally an increase in I_{K1} current will reduce cardiac excitability by opposing the stimulus current and preventing the approach toward threshold potentials. However, during reentry in CAF, the depolarizing wavefront acts as a stimulus to drive a partially excitable/recovered tissue. An increase in I_{K1} hyperpolarizes V_{rest} and causes a corresponding increase in the recovery of I_{Na} and, subsequently, the electrotonic current. The resultant enhancement of cardiac excitability causes faster spiral rotation. This mechanism also underlies the reason why a faster rotation was seen when I_{K1} was increased compared to when $I_{Ca\text{-}L}$ was blocked in CAF1 (although both showed almost similar APD shortening), since the latter did not modulate V_{rest} (Fig. 3 *C*).

The acceleration of the spirals in CAF2 is also in accordance with experimental results obtained during acetylcholine-mediated AF in sheep, where higher activation frequencies in the LA were associated with a larger density of another inward rectifier, the acetylcholine-activated K^+ current (I_{KACh}) (Sarmast et al., 2003). Thus, even though an increased I_{K1} may have a protective effect against early or late after-depolarizations at the cellular level, once AF is initiated, an increased I_{K1} will tend to stabilize rotor activity in the remodeled atrium.

Rotor termination

We simulated K^+ current blockades by decreasing the maximum conductance of the respective current under study. Our simulation results show that, unlike I_{Kr} or I_{Ks} block, I_{Kur} or I_{to} blockade successfully terminates reentry, which is potentially important for two reasons:

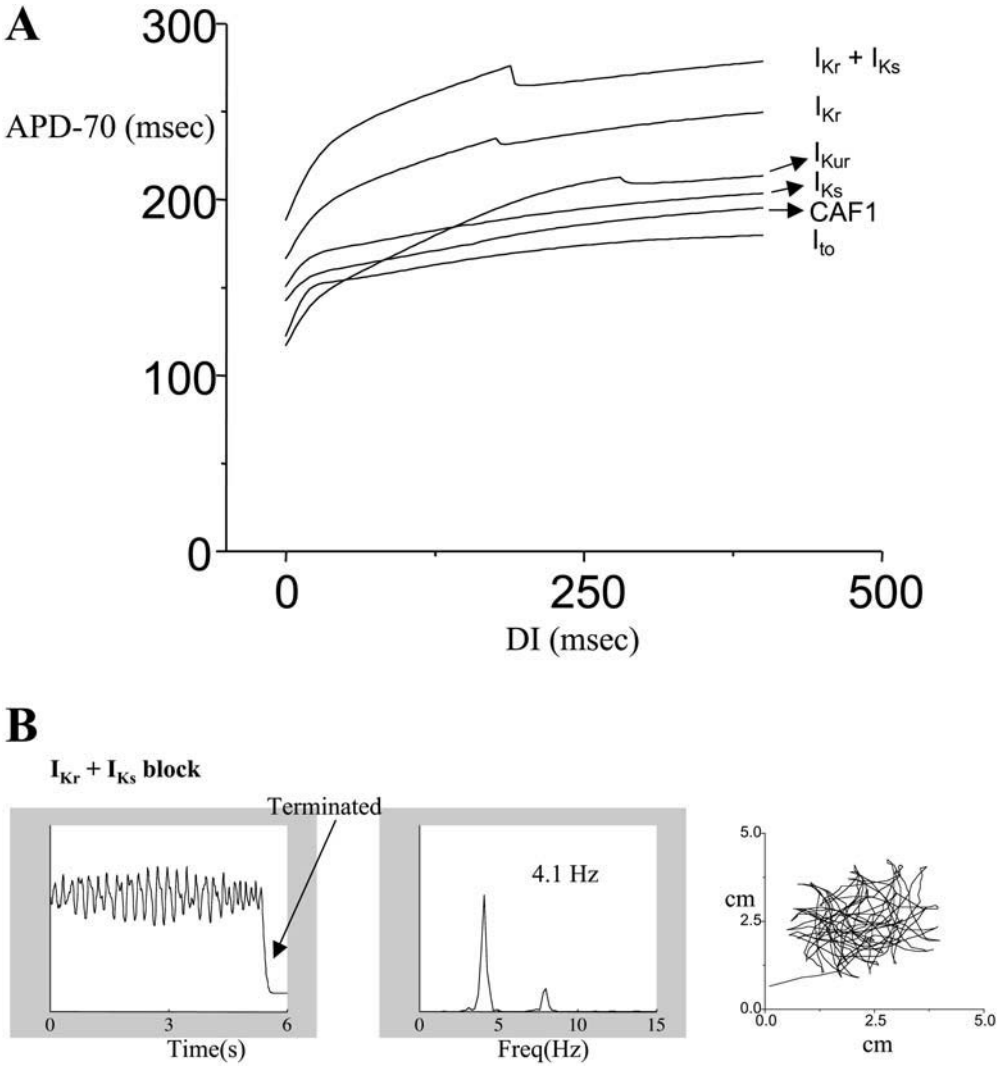

FIGURE 10 (*A*) Plot of APD restitution versus the diastolic interval (*DI*) for the CAF1 case, and in different cases of ionic current blockade. The steady-state APD was measured at –70 mV at the cellular level (at 1 Hz). (*B*) Rotor characteristics, including pseudo-ECGs, power spectral densities, and spiral-tip meander during I_{Kr} + I_{Ks} block.

1. I_{Kur} is an atrial-specific current and therefore may help avoid some of the proarrhythmic responses such as ''torsades de pointes'' associated with I_{Kr} blockade (Nattel, 1998; Nattel et al., 1999). Interestingly, recent preliminary experiments have reported the antiarrhythmic efficacy of a newly developed drug (AVE0118) in the goat model of chronic AF; this drug preferentially blocks I_{Kur} and/or I_{to} (Blaauw et al., 2004). This, in combination with our simulation results, suggests that I_{Kur} may be a useful antiarrhythmic target in chronic AF. However, we have not compared the experimental results in the goat model of chronic AF and our simulations, because a), the ionic correlates in humans and goats are different; b), rotor dynamics were not studied in the goat model; and c), the dynamics of how AVE0118 affects individual ionic currents (i.e., their state-dependent block) at the cellular level needs to be studied experimentally and via simulations first, before attempting to study their effects on rotors in 2-D simulations.
2. Our simulations also clearly show that although the largest prolongation of the APD occurs during I_{Kr} block, rotor termination actually occurs during I_{Kur}/I_{to} blockade, in which prolongation at the terminal phase is small (I_{Kur} block), or even negative (i.e., in I_{to} block, APD at the terminal phase is actually shortened; see Fig. 9), but larger at the plateau phase, and causes a wavebreak. The phenomenon of inducing wavebreaks by prolonging the plateau potential has been shown before, albeit by altering parameters of the $I_{Ca\text{-}L}$ current (Courtemanche, 1996; Xie et al., 2002). A similar phenomenon is seen in our simulations, but by blocking K^+ currents. Our results may also be clinically relevant, since a recent study showed that the APD was preferentially prolonged at the plateau potentials, when I_{Kur} current was blocked (Wettwer et al., 2004). However, the effect of prolongation of plateau potentials on rotor dynamics needs further experimental investigation.

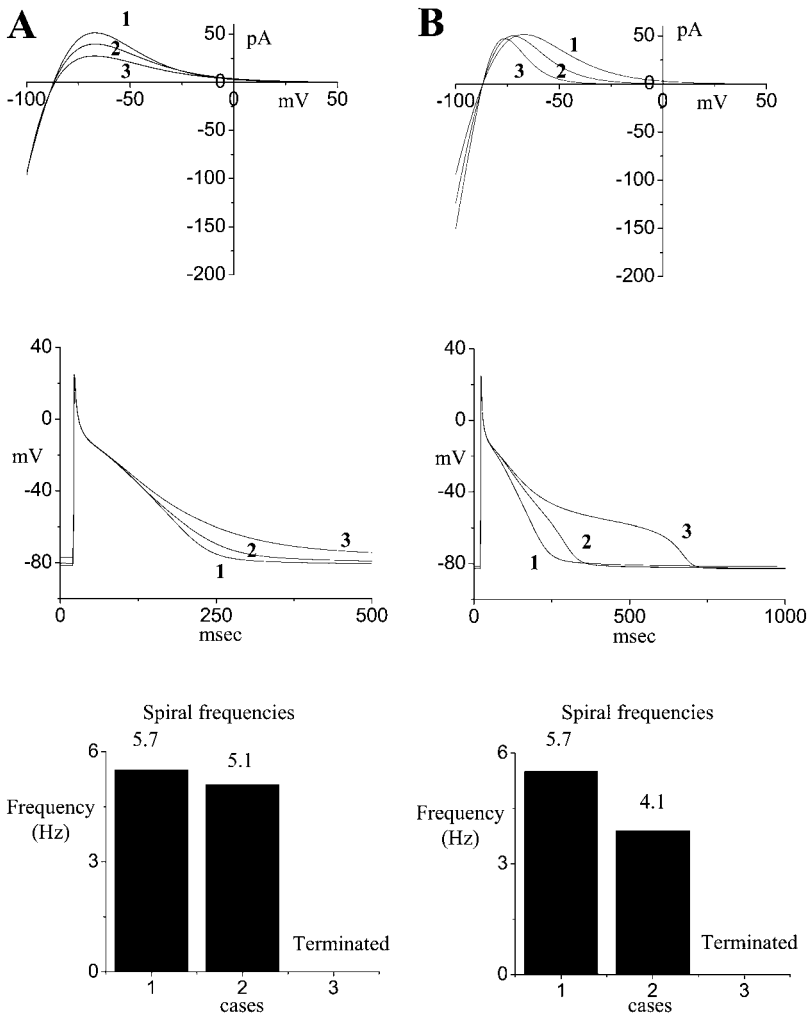

FIGURE 11 The top panel shows different cases of I_{K1} (*1*, *2*, and *3*) when (*A*) the peak outward currents were reduced, or (*B*) the outward current rectified at progressively more negative potentials. The resulting changes in the APD, and maximum spiral rotation frequencies (in CAF1) are shown below in corresponding panels.

We did not find any correlation between APD restitution and rotor termination. This, and the failure of APD prolongation at the terminal phase of repolarization to induce rotor termination below a certain threshold (i.e., I_{Kr} + I_{Ks} block) highlights the potential pitfalls in extrapolating from results obtained at the single-cell level to multicellular tissue, because the former do not account for the complex wavefront-wavetail interactions that might occur in a 2-D tissue during reentry (Beaumont et al., 1998).

Our semiquantitative analyses also suggest that understanding the mechanisms that underlie rotor pivoting will be important in predicting whether a rotor is able to self-sustain or terminates during ionic current blockade, such as during I_{Kur} block. Some of the issues underlying rotor pivoting have been addressed in earlier studies from our laboratory (Cabo et al., 1994, 1996), which demonstrated the phenomenon of vortex shedding in experiments and simulations. In these studies, wavefronts detaching from an obstacle either 1), formed a spiral wave by curling of the free end of the wavefront, or 2), proceeded into the tissue boundary and self-extinguished themselves due to decremental conduction. The behavior of the detached wavefront was determined in part by the excitability of the tissue and wavefront curvature. However, quantitative analysis of wavefront curvature and tissue excitability in complex ionic models is nontrivial and beyond the scope of this study. Hence this aspect of our modeling work should be expanded and improved upon in future studies.

Lastly, we note that even though individual blockade of I_{Kr} and I_{Ks} did not terminate the rotor, their combined block did. This case is more representative of the conventional case where APD prolongation leads to a large refractory tissue, and therefore is unable to sustain a rotor. Thus a large enough prolongation of the APD (at the terminal level) is also a viable parameter that can be targeted to terminate a rotor in the 2-D atrial substrate.

Is blockade of I_{K1} a viable antiarrhythmic option?

The feasibility of I_{K1} as a potential target for antiarrhythmic drugs arises as a natural query from the simulation results, since its density is increased in chronic AF (in contrast to the

downregulation in other K^+ currents), and because I_{K1} also significantly affects the spiral-wave dynamics. Recent experimental studies have reported the antiarrhythmic actions of β-blockers in chronic AF patients, which exerted their effects in part by increasing the input resistance of the cell, which indirectly suggests that I_{K1} was reduced (Workman et al., 2003). Our simulations show that the rotor frequencies in chronic AF are reduced not only when the peak outward I_{K1} current is reduced (Fig. 11 *A*), but also when its rectification profile is altered (Fig. 11 *B*). The motivation for the latter study comes from recent studies which indicate that the Kir2 channels that underlie I_{K1} (Kir 2.1, 2.2, and 2.3) display distinct rectification profiles (Dhamoon et al., 2004), and may be relevant since the human atrium expresses both Kir2.1 and Kir2.3 transcripts (Wang et al., 1998). The usefulness of I_{K1} blockade as an antiarrhythmic strategy has been a matter of considerable debate previously, with one of the main arguments against blocking I_{K1} current being its tendency to cause diastolic depolarization and increase the propensity for triggered arrhythmias (Kleber, 1994). However, it may be possible to overcome this difficulty by careful alterations in the rectification profile of I_{K1} (Fig. 11), and therefore we hypothesize that I_{K1} may represent an important antiarrhythmic target in persistent AF conditions.

Limitations and future studies

The limitations of the human atrial cell model used in this study are discussed elsewhere (Courtemanche et al., 1998). In addition, we utilized the ionic changes in a previous study (Courtemanche et al., 1999) to simulate the chronic AF condition in humans, since these conditions can accurately reproduce the action potential phenotype observed in chronic AF patients, i.e., a shortening of the APD, and a lack of rate dependence. However, future studies will need to take into account changes in other ionic currents, such as $I_{K,ACh}$, which has been determined to be reduced in chronic AF, and currents in which the changes remain as yet undetermined, such as I_{Kr} and I_{Ks}, as well as the Na^+/Ca^{2+} exchanger (Dobrev and Ravens, 2003). The human atrial action potential also varies considerably in its morphology and the underlying ionic currents (Benardeau et al., 1996). This can be seen when the Courtemanche atrial model is compared with another mathematical formulation for the human atrial action potential (Nygren et al., 1998). A detailed comparison between the two models can be found in a recent study (Nygren et al., 2001). Therefore, the spiral dynamics using the Nygren model in chronic AF conditions may produce different results, and requires further investigation.

Our 2-D simulations do not consider possible alterations in gap junctions, tissue anisotropy, and APD heterogeneity, all of which may play important roles in the maintenance of AF (Nattel, 2002). The issue of gap junctional remodeling in AF remains highly controversial, even experimentally (Van der Velden and Jongsma, 2002). Therefore, we have not addressed this issue at this time. Based on previous theoretical studies, we postulate that tissue anisotropy will electrically ''stretch'' the system, thereby affecting the spiral-tip trajectory, but not the period of rotation (Pertsov et al., 1993; Tung et al., 2004). The issue of APD heterogeneity and its effects on rotor maintenance were addressed in detail in a recent theoretical study, which examined the mechanism of cholinergic atrial fibrillation in a 2-D model composed of canine atrial cells (Kneller et al., 2002). Interestingly, that study also observed that in a majority of cases where AF was sustained, five out of seven cases were maintained by a dominant single spiral wave, whose underlying mechanisms was the focus of this study. Future studies could incorporate these complexities (anisotropy, gap junctions, and heterogeneity), perhaps individually or in combination, and then study the resultant effects on spiral wave maintenance and/or termination.

Finally, our present work needs to be extended to more realistic 3-D, anatomically-detailed models of the human atria, which have been formulated recently by several groups (Harrild and Henriquez, 2000; Vigmond et al., 2001; Virag et al., 2002). These models can be utilized to gain further insights into the effects of structural heterogeneities on the maintenance and/or termination of rotors.

Despite the above limitations, our results give useful and novel insights into the complex, nonlinear interactions between various ionic mechanism(s) and electrophysiological parameters that determine spiral-wave reentry in a simulated 2-D sheet of human atrial cells, under chronic AF conditions.

SUPPLEMENTARY MATERIAL

An online supplement to this article can be found by visiting BJ Online at http://www.biophysj.org.

This work was supported by grants from the National Heart, Lung, and Blood Institute (P01-HL39707, R01-HL70074, and R01-HL60843) to J.J., an American Heart Association Scientist Development Grant to O.B., an American Heart Association Post Doctoral Fellowship to S.V.P., and Canadian Institute of Health Research grant MOP 44365 to S.N.

REFERENCES

Beaumont, J., N. Davidenko, J. M. Davidenko, and J. Jalife. 1998. Spiral waves in two-dimensional models of ventricular muscle: formation of a stationary core. *Biophys. J.* 75:1–14.

Benardeau, A., S. N. Hatem, C. Rucker-Martin, B. Le Grand, L. Mace, P. Dervanian, J. J. Mercadier, and E. Coraboeuf. 1996. Contribution of Na^+/Ca^{2+} exchange to action potential of human atrial myocytes. *Am. J. Physiol.* 271:H1151–H1161.

Blaauw, Y., H. Gogelein, R. G. Tieleman, A. van Hunnik, U. Schotten, and M. A. Allessie. 2004. ''Early'' class III drugs for the treatment of atrial fibrillation: efficacy and atrial selectivity of AVE0118 in remodeled atria of the goat. *Circulation.* 110:1717–1724.

Bollmann, A., K. Sonne, H. D. Esperer, I. Toepffer, and H. U. Klein. 2002. Patients with persistent atrial fibrillation taking oral verapamil exhibit a lower atrial frequency on the ECG. *Ann. Noninvasive Electrocardiol.* 7:92–97.

Bosch, R. F., X. Zeng, J. B. Grammer, K. Popovic, C. Mewis, and V. Kuhlkamp. 1999. Ionic mechanisms of electrical remodeling in human atrial fibrillation. *Cardiovasc. Res.* 44:121–131.

Cabo, C., A. M. Pertsov, W. T. Baxter, J. M. Davidenko, R. A. Gray, and J. Jalife. 1994. Wave-front curvature as a cause of slow conduction and block in isolated cardiac muscle. *Circ. Res.* 75:1014–1028.

Cabo, C., A. M. Pertsov, J. M. Davidenko, W. T. Baxter, R. A. Gray, and J. Jalife. 1996. Vortex shedding as a precursor of turbulent electrical activity in cardiac muscle. *Biophys. J.* 70:1105–1111.

Campbell, D. L., Y. Qu, R. L. Rasmusson, and H. C. Strauss. 1993a. The calcium-independent transient outward potassium current in isolated ferret right ventricular myocytes. II. Closed state reverse use-dependent block by 4-aminopyridine. *J. Gen. Physiol.* 101:603–626.

Campbell, D. L., R. L. Rasmusson, Y. Qu, and H. C. Strauss. 1993b. The calcium-independent transient outward potassium current in isolated ferret right ventricular myocytes. I. Basic characterization and kinetic analysis. *J. Gen. Physiol.* 101:571–601.

Courtemanche, M. 1996. Complex spiral wave dynamics in a spatially distributed ionic model of cardiac electrical activity. *Chaos.* 6:579–600.

Courtemanche, M., R. J. Ramirez, and S. Nattel. 1998. Ionic mechanisms underlying human atrial action potential properties: insights from a mathematical model. *Am. J. Physiol.* 275:H301–H321.

Courtemanche, M., R. J. Ramirez, and S. Nattel. 1999. Ionic targets for drug therapy and atrial fibrillation-induced electrical remodeling: insights from a mathematical model. *Cardiovasc. Res.* 42:477–489.

de Groot, N. M., and M. A. Allessie. 2001. Mapping of atrial fibrillation. *Ann. Ist. Super. Sanita.* 37:383–392 (Review).

Dhamoon, A. S., S. V. Pandit, F. Sarmast, K. R. Parisian, P. Guha, Y. Li, S. Bagwe, S. M. Taffet, and J. M. B. Anumonwo. 2004. Unique Kir2.x properties determine regional differences in the cardiac inward rectifier K^+ current. *Circ. Res.* 94:1332–1339.

Dobrev, D., E. Graf, E. Wettwer, H. M. Himmel, O. Hala, C. Doerfel, T. Christ, S. Schuler, and U. Ravens. 2001. Molecular basis of down-regulation of G-protein-coupled inward rectifying K^+ current $I_{K,ACh}$ in chronic human atrial fibrillation: decrease in GIRK4 mRNA correlates with reduced $I_{K,ACh}$ and muscarinic receptor-mediated shortening of action potentials. *Circulation.* 104:2551–2557.

Dobrev, D., and U. Ravens. 2003. Remodeling of cardiomyocyte ion channels in human atrial fibrillation. *Basic Res. Cardiol.* 98:137–148 (Review).

Fenton, F. H., E. M. Cherry, H. M. Hastings, and S. J. Evans. 2002. Multiple mechanisms of spiral wave breakup in a model of cardiac electrical activity. *Chaos.* 12:852–892.

Franz, M. R., P. L. Karasik, C. Li, J. Moubarak, and M. Chavez. 1997. Electrical remodeling of the human atrium: similar effects in patients with chronic atrial fibrillation and atrial flutter. *J. Am. Coll. Cardiol.* 30:1785–1792.

Gray, R. A., A. M. Pertsov, and J. Jalife. 1998. Spatial and temporal organization during cardiac fibrillation. *Nature.* 392:75–78.

Harada, A., T. Konishi, M. Fukata, K. Higuchi, T. Sugimoto, and K. Sasaki. 2000. Intraoperative map guided operation for atrial fibrillation due to mitral valve. *Ann. Thorac. Surg.* 69:446–450.

Harrild, D., and C. Henriquez. 2000. A computer model of normal conduction in the human atria. *Circ. Res.* 87:E25–E36.

Jalife, J. 2000. Ventricular fibrillation: mechanisms of initiation and maintenance. *Annu. Rev. Physiol.* 62:25–50 (Review).

Jalife, J. 2003. Rotors and spiral waves in atrial fibrillation. *J. Cardiovasc. Electrophysiol.* 14:776–780.

Jalife, J., O. Berenfeld, and M. Mansour. 2002. Mother rotors and fibrillatory conduction: a mechanism of atrial fibrillation. *Cardiovasc. Res.* 54:204–216 (Review.).

Jalife, J., O. Berenfeld, A. Skanes, and R. Mandapati. 1998. Mechanisms of atrial fibrillation: mother rotors or multiple daughter wavelets, or both? *J. Cardiovasc. Electrophysiol.* 9:S2–S12 (Review).

Kim, B. S., Y. H. Kim, G. S. Hwang, H. N. Pak, S. C. Lee, W. J. Shim, D. J. Oh, and Y. M. Ro. 2002. Action potential duration restitution kinetics in human atrial fibrillation. *J. Am. Coll. Cardiol.* 39:1329–1336.

Kleber, A. G. 1994. I_{K1} blockade as an antiarrhythmic mechanism. *Cardiovasc. Res.* 28:720.

Kneller, J., R. Zou, E. J. Vigmond, Z. Wang, L. J. Leon, and S. Nattel. 2002. Cholinergic atrial fibrillation in a computer model of a two-dimensional sheet of canine atrial cells with realistic ionic properties. *Circ. Res.* 90:E73–E87.

Liu, S., and R. L. Rasmusson. 1997. Hodgkin-Huxley and partially coupled inactivation models yield different voltage dependence of block. *Am. J. Physiol.* 272:H2013–H2022.

Moe, G. K. 1962. On the multiple wavelet hypothesis of atrial fibrillation. *Arch. Int. Pharmacodyn. Ther.* 140:183–188.

Nattel, S. 1998. Experimental evidence for proarrhythmic mechanisms of antiarrhythmic drugs. *Cardiovasc. Res.* 37:567–577 (Review).

Nattel, S. 2002a. New ideas about atrial fibrillation 50 years on. *Nature.* 415:219–226.

Nattel, S., P. Khairy, D. Roy, B. Thibault, P. Guerra, M. Talajic, and M. Dubuc. 2002b. New approaches to atrial fibrillation management: a critical review of a rapidly evolving field. *Drugs.* 62:2377–2397.

Nattel, S., L. Yue, and Z. Wang. 1999. Cardiac ultrarapid delayed rectifiers: a novel potassium current family of functional similarity and molecular diversity. *Cell. Physiol. Biochem.* 9:217–226 (Review).

Nygren, A., C. Fiset, L. Firek, J. W. Clark, D. S. Lindblad, R. B. Clark, and W. R. Giles. 1998. Mathematical model of an adult human atrial cell: the role of K^+ currents in repolarization. *Circ. Res.* 82:63–81.

Nygren, A., L. J. Leon, and W. R. Giles. 2001. Simulations of the human atrial action potential. *Philos. Trans. Roy. Soc. Lond. A.* 359:1111–1125.

Pertsov, A. M., J. M. Davidenko, R. Salomonsz, W. T. Baxter, and J. Jalife. 1993. Spiral waves of excitation underlie reentrant activity in isolated cardiac muscle. *Circ. Res.* 72:631–650.

Sahadevan, J., K. Ryu, L. Peltz, C. M. Khrestian, R. W. Stewart, A. H. Markowitz, and A. L. Waldo. 2004. Epicardial mapping of chronic atrial fibrillation in patients: preliminary observations. *Circulation.* 110:3293–3299.

Samie, F. H., O. Berenfeld, J. Anumonwo, S. F. Mironov, S. Udassi, J. Beaumont, S. M. Taffet, A. M. Pertsov, and J. Jalife. 2001. Rectification of the background potassium current: a determinant of rotor dynamics in ventricular fibrillation. *Circ. Res.* 89:1216–1223.

Samie, F. H., R. Mandapati, R. A. Gray, Y. Watanabe, C. Zuur, J. Beaumont, and J. Jalife. 2000. A mechanism of transition from ventricular fibrillation to tachycardia: effect of calcium channel blockade on the dynamics of rotating waves. *Circ. Res.* 86:684–691.

Sarmast, F., A. Kolli, A. Zaitsev, K. Parisian, A. S. Dhamoon, P. K. Guha, M. Warren, J. M. Anumonwo, S. M. Taffet, O. Berenfeld, and J. Jalife. 2003. Cholinergic atrial fibrillation: $I_{K,ACh}$ gradients determine unequal left/right atrial frequencies and rotor dynamics. *Cardiovasc. Res.* 59:863–873.

Scheinman, M. M., and F. Morady. 2001. Nonpharmacological approaches to atrial fibrillation. *Circulation.* 103:2120–2125.

Skanes, A. C., R. Mandapati, O. Berenfeld, J. M. Davidenko, and J. Jalife. 1998. Spatiotemporal periodicity during atrial fibrillation in the isolated sheep heart. *Circulation.* 98:1236–1248.

Sticherling, C., W. Hsu, H. Tada, A. C. Bares, H. Oral, F. Pelosi, B. P. Knight, S. A. Strickberger, and F. Morady. 2002. Effects of verapamil and ibutilide on atrial fibrillation and postfibrillation atrial refractoriness. *J. Cardiovasc. Electrophysiol.* 13:151–157.

Tung, L., N. Bursac, and F. Aguel. 2004. Rotors and spiral waves in two dimensions. *In* Cardiac Electrophysiology: From Cell to Bedside, 4th ed. D. Zipes and J. Jalife, editors. Saunders, Philadelphia. 336–344.

Van der Velden, H. M., and H. J. Jongsma. 2002. Cardiac gap junctions and connexins: their role in atrial fibrillation and potential as therapeutic targets. *Cardiovasc. Res.* 54:270–279.

Van Wagoner, D. R., A. L. Pond, P. M. McCarthy, J. S. Trimmer, and J. M. Nerbonne. 1997. Outward K^+ current densities and Kv1.5 expression are reduced in chronic human atrial fibrillation. *Circ. Res.* 80:772–781.

Vigmond, E. J., R. Ruckdeschel, and N. Trayanova. 2001. Reentry in a morphologically realistic atrial model. *J. Cardiovasc. Electrophysiol.* 12:1046–1054.

Virag, N., V. Jacquemet, C. S. Henriquez, S. Zozor, O. Blanc, J. M. Vesin, E. Pruvot, and L. Kappenberger. 2002. Study of atrial arrhythmias in a computer model based on magnetic resonance images of human atria. *Chaos.* 12:754–763.

Wang, Z., L. Yue, M. White, G. Pelletier, and S. Nattel. 1998. Differential distribution of inward rectifier potassium channel transcripts in human atrium versus ventricle. *Circulation.* 98:2422–2428.

Warren, M., P. K. Guha, O. Berenfeld, A. Zaitsev, J. M. Anumonwo, A. S. Dhamoon, S. Bagwe, S. M. Taffet, and J. Jalife. 2003. Blockade of the inward rectifying potassium current terminates ventricular fibrillation in the guinea pig heart. *J. Cardiovasc. Electrophysiol.* 14: 621–631.

Wettwer, E., O. Hala, T. Christ, J. F. Heubach, D. Dobrev, M. Knaut, A. Varro, and U. Ravens. 2004. Role of I_{Kur} in controlling action potential shape and contractility in the human atrium: influence of chronic atrial fibrillation. *Circulation.* 110:2299–2306.

Workman, A. J., K. A. Kane, J. A. Russell, J. Norrie, and A. C. Rankin. 2003. Chronic beta-adrenoceptor blockade and human atrial cell electrophysiology: evidence of pharmacological remodelling. *Cardiovasc. Res.* 58:518–525.

Xie, F., Z. Qu, A. Garfinkel, and J. N. Weiss. 2002. Electrical refractory period restitution and spiral wave reentry in simulated cardiac tissue. *Am. J. Physiol. Heart Circ. Physiol.* 283:H448–H460.